Monthly Notices
of the
ROYAL ASTRONOMICAL SOCIETY

MNRASL **445,** L65–L69 (2014) doi:10.1093/mnrasl/slu138

Environmental dependence of star formation induced by cloud collisions in a barred galaxy

Yusuke Fujimoto, Elizabeth J. Tasker★ and Asao Habe

Department of Physics, Faculty of Science, Hokkaido University, Kita 10, Nisi 8, Kita-ku, Sapporo 060-0810, Japan

Accepted 2014 August 20. Received 2014 August 20; in original form 2014 August 4

ABSTRACT

Cloud collision has been proposed as a way to link the small-scale star formation process with the observed global relation between the surface star formation rate and gas surface density. We suggest that this model can be improved further by allowing the productivity of such collisions to depend on the relative velocity of the two clouds. Our adjustment implements a simple step function that results in the most successful collisions being at the observed velocities for triggered star formation. By applying this to a high-resolution simulation of a barred galaxy, we successfully reproduce the observational result that the star formation efficiency (SFE) in the bar is lower than that in the spiral arms. This is not possible when we use an efficiency dependent on the internal turbulence properties of the clouds. Our results suggest that high-velocity collisions driven by the gravitational pull of the clouds are responsible for the low bar SFE.

Key words: hydrodynamics – methods: numerical – ISM: clouds – ISM: structure – galaxies: star formation – galaxies: structure.

1 INTRODUCTION

Recent studies of galactic-scale star formation have revealed that the rate at which stars are produced depends on the galactic environment. Global structures within a galaxy result in changes to the star formation rates (SFR), even when the gas surface density is almost the same. In observations of disc galaxies, the star formation efficiency (SFE $= \Sigma_{\rm SFR}/\Sigma_{\rm gas}$) is found to vary between the nucleus and disc region (Muraoka et al. 2007), and between the arm and inter-arm (Muraoka et al. 2009; Hirota et al. 2014).

High-resolution (∼250 pc) ^{12}CO($J = 1$–0) observations of the barred galaxy M61 (NGC 4303) by Momose et al. (2010) showed that the SFE in the bar is 50 per cent of that in the spiral arms. Previous studies have suggested that this drop is due to strong shear along the bar that provides a turbulence injection to support the giant molecular clouds (GMCs; Tubbs 1982; Athanassoula 1992; Downes et al. 1996; Reynaud & Downes 1998; Sorai et al. 2012; Meidt et al. 2013). However, there is counter evidence suggesting that the role of shear is too small to be consequential to the evolution of the GMCs. For clouds in our own Galaxy, Dib et al. (2012) found that shear is consistently a fraction of the value needed to disrupt a density perturbation, and thereby does not affect star formation.

A way to resolve this disparage is to use simulations, yet here too there is disagreement. In two-dimensional models of the barred galaxy M83, Nimori et al. (2012) found that the SFE in the bar region was 60 per cent of the spiral arm due to the strong internal turbulence of the clouds. Conversely, more recent 3D models of the same galaxy performed by Fujimoto et al. (2014) found that the typical internal cloud velocity dispersion showed little variation between clouds forming in the bar, spiral arm and disc. This implied shear might not be the key to understanding the varying SFR. Yet, the situation is complicated by the SFE being highly dependent on the stellar model used.

Fujimoto et al. (2014) did not include active star formation, but estimated the SFE based on the gas properties. There are multiple methods for doing this, each based on assumptions as to what governs the production of stars. Two methods used by Fujimoto et al. (2014) compared a scheme utilizing the internal properties of the cloud with one that considered star formation driven by cloud interactions. The former was proposed by Krumholz & McKee (2005) and assumed that clouds are supersonically turbulent with a log-normal density distribution. By demanding that gas collapses when the gravitational energy within a cloud exceeds its turbulent energy, they find that the SFR per cloud is

$$\mathrm{SFR_c} = \epsilon_{\rm ff} \left(\frac{\alpha_{\rm vir}}{1.3}\right)^{-0.68} \left(\frac{\mathcal{M}}{100}\right)^{-0.32} \frac{M_{\rm c}}{t_{\rm ff}}, \quad (1)$$

where the star formation efficiency per free-fall time $\epsilon_{\rm ff} = 0.014$, the virial parameter $\alpha_{\rm vir} = 5\sigma_{\rm c}^2 R_{\rm c}/GM_{\rm c}$, properties $R_{\rm c}$, $M_{\rm c}$ and $\sigma_{\rm c}$ are the cloud radius, mass and 1D velocity dispersion, the Mach number is the ratio between the cloud's velocity dispersion and the sound speed, $\mathcal{M} \equiv \sigma_{\rm c}/c_{\rm s}$, and $t_{\rm ff}$ is the cloud free-fall time.

The second scheme assumes that star formation is initiated by collisions between clouds. Such interactions can trigger a shock at

★ E-mail: yusuke@astro1.sci.hokudai.ac.jp

the collision interface which fragments into stars. This has been suggested as a way to unite the local star formation process with the globally observed Kennicutt–Schmidt relation (Kennicutt 1998; Tan 2000; Tasker & Tan 2009) and also as a mechanism to create massive stars and super star clusters (Habe & Ohta 1992; Furukawa et al. 2009; Ohama et al. 2010; Dib et al. 2013; Fukui et al. 2014; Takahira, Tasker & Habe 2014). Since there is evidence that clouds may be gravitationally unbound (Heyer et al. 2009; Dobbs, Burkert & Pringle 2011), cloud collisions could be the best candidate to create the dense regions where stars are formed. In the shock-generating model proposed by Tan (2000), the surface density of the SFR becomes

$$\Sigma_{\rm SFR} = \frac{\epsilon f_{\rm sf} N_{\rm A} M_{\rm c}}{t_{\rm coll}}, \quad (2)$$

where $\epsilon = 0.2$ is the total fraction of cloud gas converted to stars during a star-forming collision, $f_{\rm sf}$ is the fraction of cloud collisions which successfully lead to star formation, $N_{\rm A}$ is the surface number density of clouds, $M_{\rm c}$ is the cloud mass and $t_{\rm coll}$ is the typical time between collisions.

Fujimoto et al. (2014) found that neither of these models produced the observed lower SFE in the bar region. With the turbulence model in equation (1), the SFE was equal in the bar and spiral arms, while the cloud collision model in equation (2) gave a higher SFE in the bar than the arms. The first of these was consistent with the result that the typical cloud properties were not dependent on cloud environment. The cloud collision model reflected the fact that the collision rate was highest in the densely packed bar environment, leading to a higher SFR. In this case, the difference in the galactic environment produced the opposite effect to that in observations, but this might have been due to a simplification made in equation (2).

The cloud collision model assumes that all collisions are equally likely to produce star formation. The fractional success rate, $f_{\rm sf}$, is taken to be constant whose value was selected to be 0.5 in Fujimoto et al. (2014). This approximation is known to be inaccurate. In observations of triggered star formation in cloud collisions by Fukui et al. (2014), Ohama et al. (2010) and Furukawa et al. (2009), the formation of super star clusters was found to be associated with collisional velocities around 20 km s^{-1}. This was investigated in simulations by Takahira et al. (2014), who found that the production of star-forming cores in a collision strongly depended on the relative velocity of the two clouds. A slow collision would not produce a shock strong enough to create a dense region at the cloud interface while too fast a collision would result in the shock front exiting the cloud before a core had time to form. The value of $f_{\rm sf}$ should therefore depend on the relative velocity of the colliding clouds.

To be strictly accurate, the values for $f_{\rm sf}$ and ϵ are not independent. If $f_{\rm sf}$ depends on velocity, then a prime velocity for production of stars is going to produce a higher efficiency. However, for the sake of simplicity, we consider ϵ to represent the average conversion efficiency and assume that only $f_{\rm sf}$ varies. We keep the value of ϵ suggested in Tan (2000) as 0.2.

In this Letter, we calculate the SFE in the barred galaxy model of Fujimoto et al. (2014) using a revised version of the cloud collision star formation scheme in equation (2), accounting for variations in stellar production due to the collisional velocity of the clouds. We compare the results in different galactic regions of the simulation with those in observations.

2 SIMULATION

The simulation presented in this Letter was run using ENZO: a 3D adaptive mesh refinement hydrodynamics code (The Enzo Collaboration 2013). Our galaxy was modelled on the nearby barred spiral galaxy, M83, with the gas distribution and stellar potential taken from observational results. For the galaxy's radial gas distribution, we assumed an initial exponential density profile based on the observations of Lundgren et al. (2004) and used fixed-motion star particles to create a stellar potential with the observed pattern speed for M83.

The GMCs in our simulation were identified as coherent structures contained within contours at a threshold density of $n_{\rm H,c} = 100$ cm^{-3}, similar to the observed mean volume densities of typical galactic GMCs. The simulation outputs were analysed every 1 Myr and the clouds mapped between consecutive times. This cloud tracking algorithm is described in Tasker & Tan (2009). A collision is said to have happened when a single cloud is at the predicted position for two other clouds after 1 Myr of evolution. It is a lower estimate of the true cloud interaction rate, since it does not include tidal shredding where two identifiable objects exist at the end of the encounter.

After 120 Myr (one pattern rotation period), the gas is fully fragmented, and between 200 Myr and 280 Myr, the galactic disc settles into a quasi-equilibrium with no large structural change. We analysed the clouds at 240 Myr.

We assigned an environment group based on the cloud's physical location within the disc. If a cloud is found within the galactic radii $2.5 < r < 7.0$ kpc, it is recognized as a spiral cloud. Outside $r = 7.0$ kpc, clouds are designated disc clouds. Bar clouds form in a box-like region at the galactic centre, with a length of 5.0 kpc and width 1.2 kpc. The nucleus region inside 600 pc is excluded due to the difficulty in accurately tracking clouds in such a high-density area. The boundaries of these three regions are shown in fig. 5 of Fujimoto et al. (2014), along with a more thorough description of the simulation.

3 RESULTS

3.1 Environmental dependence of collision velocity

In order to determine whether collision velocity is likely to play a role in the productiveness of triggered star formation, we looked at the range of values present in the simulation. Fig. 1 shows the collision velocity distribution in each of our three galactic regions. This was calculated from the relative velocity of the clouds 1 Myr prior to their merger, $v_{\rm coll} = |\boldsymbol{v}_1 - \boldsymbol{v}_2|$, where $\boldsymbol{v}_1$ and $\boldsymbol{v}_2$ are the bulk velocities of the clouds. Since the number of collisions occurring in a 1 Myr output interval is small, we included all collisions occurring between $t = 230$ and 240 Myr, during the quiescent period of the disc's evolution.

The collision velocity shows a clear dependence on the galactic environment. The bar region has the widest range, extending out to 120 km s^{-1} with only a small peak in the distribution around 35 km s^{-1}. By contrast, the spiral region has a steeped profile with a typical collision speed of 20 km s^{-1} and clouds rarely colliding faster than 60 km s^{-1}. In the disc region, interactions are more gentle with a collision speed peaking at only 15 km s^{-1} and a maximum of 40 km s^{-1}.

By virtue of its area, the total number of cloud collisions is highest in the spiral region. However, the fraction of clouds undergoing a collision event is higher in the bar, due to the constrained elliptical

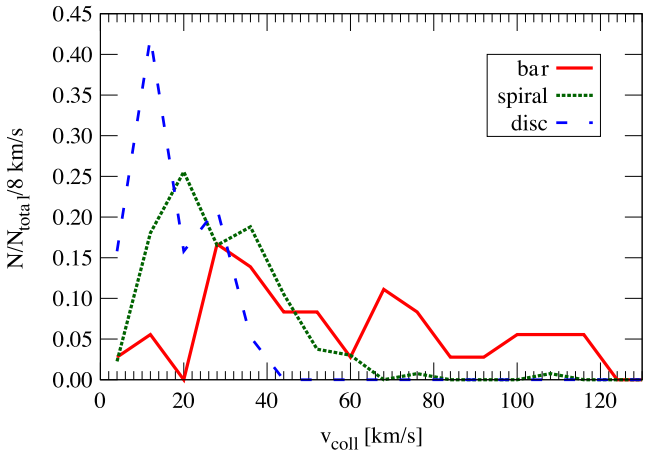

Figure 1. Distribution of the collision velocity of clouds colliding in the bar region (solid red line), spiral region (dotted green line) and disc region (dashed blue line). The collision events are counted for 10 Myr from $t = 230$ to 240 Myr.

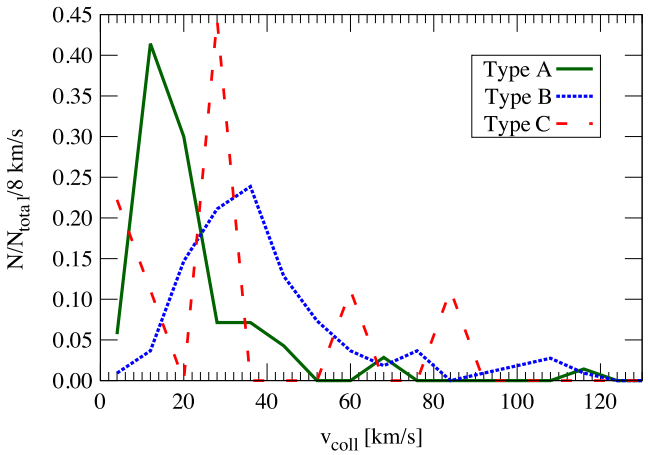

Figure 2. Distribution of the collision velocity for three cloud categorisations: type A (solid green line) are the most common clouds with properties typical of observed GMCs, type B (dotted blue line) are massive associations and type C (dashed red line) are unbound, transient clouds. The cloud type plotted is that of the most massive cloud involved in the collision.

motion. This bolstered rate of interaction alters the properties of the clouds, allowing much larger structures to be built through successive mergers. The result is a group of giant molecular associations (GMAs) that dominate the local gravitational field, pulling clouds on to a collision course that increases their relative velocity.

That the collision velocity can be attributed to properties of the cloud population can be seen clearly in Fig. 2. The collision velocity is now plotted for three different types of cloud, categorized by their mass and radius. type A clouds form the main population in the disc. Their properties are consistent with observed GMCs with masses $\sim 5 \times 10^5$ $M_\odot$ and radii $\sim$11 pc. type B clouds are the giant GMAs with masses above 10^6 $M_\odot$. type C clouds are unbound objects that have short lives in filaments and the tidal tails of larger interacting clouds. The cloud type was determined using the mass–radius relation described in detail in Fujimoto et al. (2014), and the collision cloud type is dictated by the largest object of the interacting pair, resulting in a low number of type C with a noisy distribution. These distributions show that collisions involving a GMA type B cloud are faster. The speed peaks around 40 km s^{-1} and extends to beyond 100 km s^{-1}. By contrast, a typical collision with a type A cloud occurs at half the speed of those with type B. This fast interaction speed for the type B is consistent with their escape velocity, which ranges between 17 and 100 km s^{-1} for the clouds with masses between 10^6and10^8 $M_\odot$ and radii 30 and 100 pc. The type B clouds form a dominant population in the bar as shown in Table 1. Half the clouds in the bar are either type B or the small type C forming in the interaction tails of the type B. The spiral and disc region have a stronger population of type A clouds, with the disc having less than 6 per cent type B. The type B clouds therefore govern the interactions in the bar, producing a higher collision speed than either the spiral or the disc. This supports the idea that the variation in SFE with galactic region might be due to a variation in the efficiency of triggered star formation.

3.2 Environmental dependence of SFE

To equate the cloud collision rate to the SFR, we used the model proposed by Tan (2000) in equation (2) to plot the observed Kennicutt–Schmidt relation between the surface SFR density and surface gas density. We calculated the surface area in the x–y plane (face-on disc) and averaged the data over cylindrical regions with height 5 kpc and radius 500 pc, in keeping with the typical observational resolution. If we assume that a constant fraction of all collisions lead to star formation with $f_{\rm sf} = 0.5$ in equation (2), we obtain the Kennicutt–Schmidt relation in the left-hand panel of Fig. 3. The SFE is proportional to the frequency of collisions, with the bar having the highest number of cloud collisions and therefore the highest efficiency.

In order to take into account the dependence of $f_{\rm sf}$ on the collision velocity, we use the step function described in Table 2. Since observations of triggered star formation found a collision velocity around $\sim$20 km s^{-1} (Furukawa et al. 2009; Ohama et al. 2010; Fukui et al. 2014), we assume that collisions between 10 and 40 km s^{-1} are ideally suited to creating stars and set $f_{\rm sf} = 0.5$ in this range. This is consistent with the majority of our collisions in Fig. 1, a necessity since the average SFR is in good agreement with observations (Bigiel et al. 2008). Outside this region, we assume that a collision velocity less than 10 km s^{-1} is too slow to form the compressed shock front that leads to efficient star formation while velocities higher than 40 km s^{-1} produce interaction times between clouds that are too short to form a high number of stars. Within these

Table 1. The percentage of each cloud type in each galactic region at $t = 240$ Myr. Numbers in parentheses show the actual number of clouds of that type divided by the total cloud number in the region.

	Bar	Spiral	Disc
Type A	49.4 per cent (38/77)	64.1 per cent (330/515)	83.3 per cent (85/102)
Type B	13.0 per cent (10/77)	12.8 per cent (66/515)	5.9 per cent (6/102)
Type C	37.7 per cent (29/77)	23.1 per cent (119/515)	10.8 per cent (11/102)

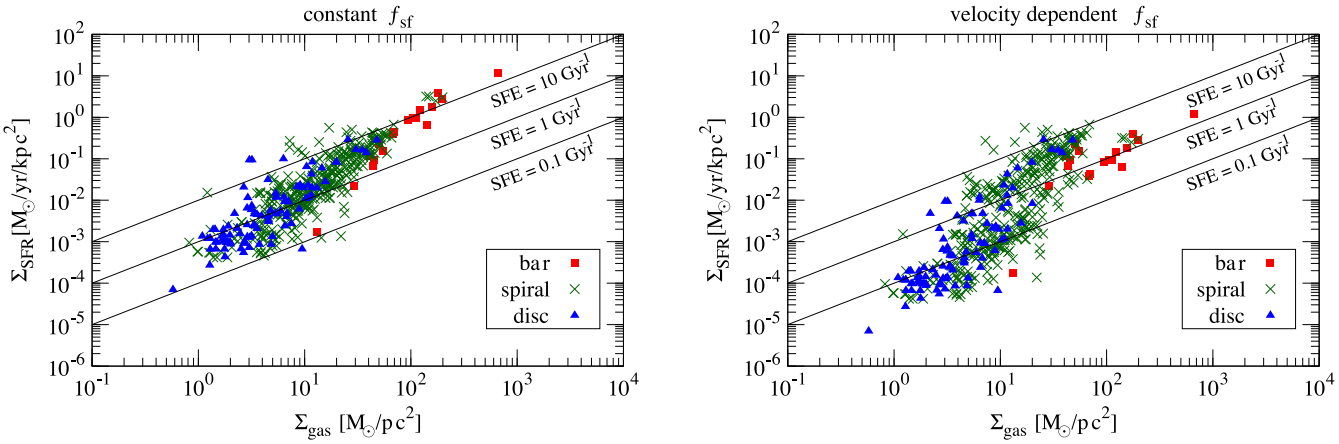

Figure 3. Relation between gas surface density and SFR surface density. The SFR is estimated by the cloud collision model depending on the average collision velocity in 500 pc × 5 kpc cylindrical regions. The left-hand panel uses a constant f_{sf} while the right-hand panel uses the collision velocity-dependent f_{sf}, as described in Table 2. The coloured markers denote different galactic regions: red squares are clouds in the bar region, green crosses are for the spiral region and blue triangles are those in the disc region. The black solid lines show constant SFEs = 10, 1, 0.1 Gyr^{-1}.

Table 2. The fraction of collisions that result in star formation, f_{sf}, for different collision velocities, v_{coll}.

v_{coll}	$0 \sim 10$ km s^{-1}	$10 \sim 40$ km s^{-1}	40 km s^{-1} $\sim$
f_{sf}	0.05	0.5	0.05

ranges, we therefore lower the value of f_{sf} by a factor of 10. Exactly where these cutoffs should be and the correct value for f_{sf} requires a further exploration of shock speed and cloud structure, so here we select values that lie within our observed range of velocities and agreed with the observations available.

The result of including this collision velocity dependence is shown in the right-hand panel of Fig. 3. With a significant fraction of the bar clouds colliding at high velocities with a low success rate, the SFE in this region drops. This produces a lower SFE in the bar than a large fraction of the spiral regions, in agreement with the observations of Momose et al. (2010), where the bar SFE lies in the lower half of the SFE spread in the spiral. The spiral region shows an increased range of efficiencies due to its broad profile of collision velocities in Fig. 1 having tails in both our low-efficiency regions. Conversely, most of the disc clouds collide too slowly for strong star formation, decreasing the efficiency of the majority of these points. This demonstrates that while the cloud collision model for star formation can successfully reproduce the Kennicutt–Schmidt relation, the dependence on the velocity of the interaction introduces an environmental dependence that cannot be ignored.

A second comparison point is that the radial distribution of the SFE was measured by Hirota et al. (2014) for the bar region in M83. They found a peak in the SFE at the bar end, corresponding to an efficiency of ∼2 Gyr^{-1} which drops to ∼0.3 Gyr^{-1} along the bar length. We compared this to the radial profiles we obtain using the cloud collision and turbulence models for SFE in Fig. 4. For star formation estimated from the cloud turbulence in equation (1), there is no radial dependence and we see a constant efficiency through the three galaxy environments. Using the velocity-dependent collision scheme, a clear drop is seen after the bar end of the same magnitude as in the observations.

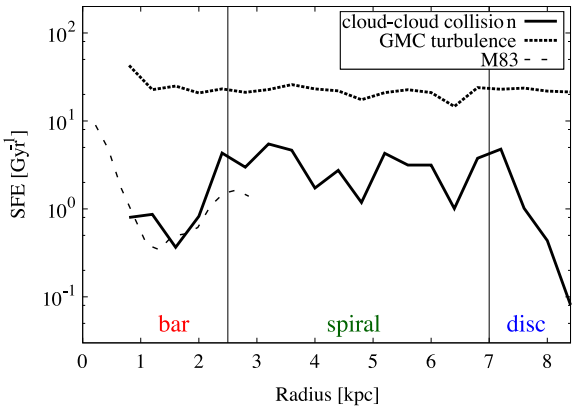

Figure 4. Azimuthally averaged (bin size 400 pc) radial distributions of the SFE estimated by the velocity-dependent cloud collision model (solid line), the cloud turbulence model (dashed line) and from observations of M83 by Hirota et al. (2014, wide dashes). The vertical lines show the borders of galactic regions: 600 pc $< r <$ 2.5 kpc marks the bar region, 2.5 $< r <$ 7.0 kpc is the spiral region and $r >$ 7.0 kpc is the disc region.

4 CONCLUSION

We investigated the variation in the relative velocity of cloud collisions in different regions of a simulated galaxy. Using this, we proposed a change to the triggered star formation model developed by Tan (2000) that varied the effectiveness of star formation from cloud collisions based on the speed at which the clouds collide. Taking the observations of triggered star formation as the most successful velocity for forming stars, we varied the fraction of collisions that would result in star formation such that collisions between 10 and 40 km s^{-1} were successful 50 per cent of the time, while collisions slower and faster than this range were only successful 5 per cent of the time. Our main results are as follows.

(i) The collision velocity shows a clear dependence on galactic environment. Clouds formed in the bar region typically collide faster than those in the spiral. Clouds in the disc are involved in the gentlest collisions.

(ii) This dependence is due to the distribution of cloud types in the three regions. A higher fraction of bar clouds are massive, creating strong gravitational interactions that increase the collision velocity.

(iii) The unproductive collisions in the bar region lower the SFE to put it below the maximum efficiency in the spiral region. This is despite collisions being more common in the bar region. The result is in agreement with observations of other barred galaxies.

(iv) When plotted as a radial distribution, the drop in SFE at the bar end is also consistent with observational measurements of M83. This is not reproduced when the SFE is calculated from the cloud turbulence, which shows a constant SFE across all regions.

One area not considered is the effect of stellar feedback. The impact of feedback is a hot topic, with opinions suggesting that it does not affect the GMCs (Renaud et al. 2013) implying that it is a controlling force. In stellar wind models performed by Dib et al. (2013), the SFE in a star-forming clump decreased with clump mass. Such an effect could also explain the lower bar SFE if the larger GMAs resulted in more massive clumps. However, the authors also find that for star clusters thought to be formed in cloud collisions, the best-fitting model uses an increasing SFR with time. This is likely to be controlled by the evolution of the collision-induced surface density, which Takahira et al. (2014) demonstrated depends strongly on collision speed. The two effects will therefore work in parallel and further investigation is needed to separate out their contributions.

ACKNOWLEDGEMENTS

The authors would like to thank the YT development team (Turk et al. 2011) for help during the analysis of these simulations. Numerical computations were carried out at the Center for Computational Astrophysics (CfCA) of the National Astronomical Observatory of Japan. EJT is funded by the MEXT grant for the Tenure Track System and the Suhara Memorial Foundation.

REFERENCES

Athanassoula E., 1992, MNRAS, 259, 345
Bigiel F., Leroy A., Walter F., Brinks E., de Blok W. J. G., Madore B., Thornley M. D., 2008, AJ, 136, 2846
Dib S., Helou G., Moore T. J. T., Urquhart J. S., Dariush A., 2012, ApJ, 758, 125
Dib S., Gutkin J., Brandner W., Basu S., 2013, MNRAS, 436, 3727
Dobbs C. L., Burkert A., Pringle J. E., 2011, MNRAS, 413, 2935
Downes D., Reynaud D., Solomon P. M., Radford S. J. E., 1996, ApJ, 461, 186
Fujimoto Y., Tasker E. J., Wakayama M., Habe A., 2014, MNRAS, 439, 936
Fukui Y. et al., 2014, ApJ, 780, 36
Furukawa N., Dawson J. R., Ohama A., Kawamura A., Mizuno N., Onishi T., Fukui Y., 2009, ApJ, 696, L115
Habe A., Ohta K., 1992, PASJ, 44, 203
Heyer M., Krawczyk C., Duval J., Jackson J. M., 2009, ApJ, 699, 1092
Hirota A. et al., 2014, PASJ, 66, 46
Kennicutt R. C., Jr, 1998, ApJ, 498, 541
Krumholz M. R., McKee C. F., 2005, ApJ, 630, 250
Lundgren A. A., Wiklind T., Olofsson H., Rydbeck G., 2004, A&A, 413, 505
Meidt S. E. et al., 2013, ApJ, 779, 45
Momose R., Okumura S. K., Koda J., Sawada T., 2010, ApJ, 721, 383
Muraoka K. et al., 2007, PASJ, 59, 43
Muraoka K. et al., 2009, ApJ, 706, 1213
Nimori M. et al., 2012, MNRAS, 429, 2175
Ohama A. et al., 2010, ApJ, 709, 975
Renaud F. et al., 2013, MNRAS, 436, 1836
Reynaud D., Downes D., 1998, A&A, 337, 671
Sorai K. et al., 2012, PASJ, 64, 51
Takahira K., Tasker E. J., Habe A., 2014, ApJ, 792, 63
Tan J. C., 2000, ApJ, 536, 173
Tasker E. J., Tan J. C., 2009, ApJ, 700, 358
Bryan G. L. et al. The Enzo Collaboration:, 2013, ApJS, 211, 19
Tubbs A. D., 1982, ApJ, 255, 458
Turk M. J., Smith B. D., Oishi J. S., Skory S., Skillman S. W., Abel T., Norman M. L., 2011, ApJS, 192, 9

This paper has been typeset from a TEX/LATEX file prepared by the author.